ACS Catalysis

RESEARCH ARTICLE

pubs.acs.org/acscatalysis

Highly Dispersed Pd-SBA15 Materials from Tris(*tert*-butoxy)siloxy Complexes of Pd(II)

Yeon S. Choi,[†,∥] Eric G. Moschetta,[‡] Jeffrey T. Miller,[§] Meg Fasulo,[∥,⊥] Meredith J. McMurdo,[∥,⊥] Robert M. Rioux,*[,‡] and T. Don Tilley*[,∥,⊥]

[†]Department of Chemical & Biomolecular Engineering and [∥]Department of Chemistry, University of California, Berkeley, Berkeley, California 94720, United States

[‡]Department of Chemical Engineering, The Pennsylvania State University, University Park, Pennsylvania 16802, United States

[§]Chemical Sciences and Engineering Division, Argonne National Laboratory, Argonne, Illinois 60439, United States

[⊥]Chemical Sciences Division, Lawrence Berkeley National Laboratory, 1 Cyclotron Road, Berkeley, California 94720, United States

Supporting Information

ABSTRACT: Two novel tris(*tert*-butoxy)siloxy palladium (II) complexes of the form (4,4′-di-*tert*-butyl-2,2′-bipyridyl)Pd-[OSi(O^{t}Bu)$_3$](R) were synthesized (**1**, R = OSi(O^{t}Bu)$_3$ and **2**, R = CH$_3$). The structures of these compounds were determined by multinuclear NMR spectroscopy and single crystal X-ray diffraction. The solid-state thermolytic chemistry of **1** and **2** was studied by thermogravimetric analysis (TGA) and differential scanning calorimetry (DSC). These compounds were covalently grafted onto the surface of mesoporous silica (SBA15) under mild, nonaqueous conditions to generate supported Pd(II) centers. Reactions of **1** and **2** with the surface Si−OH groups occurs selectively through the -OSi(O^{t}Bu)$_3$ ligand with elimination of HOSi(O^{t}Bu)$_3$. The new materials, designated **Pd(1)SBA15** and **Pd(2)SBA15**, were characterized using N_2 porosimetry, TGA, powder X-ray diffraction (PXRD), X-ray absorption spectroscopy (XAS), and transmission electron microscopy (TEM). The coordination environments of the supported Pd centers were investigated using Fourier-transform infrared (FTIR) spectroscopy, diffuse reflectance UV−vis (DRUV−vis) spectroscopy, and XAS. Comparison with the molecular precursors **1** and **2** revealed that the supported Pd centers share many of the same structural and spectroscopic characteristics. The supported Pd centers were robust in inert atmosphere up to the decomposition temperatures of **1** and **2** (150−200 °C). The catalytic behavior of the **PdSBA15** materials in the semihydrogenation of 1-phenyl-1-propyne was studied and compared to that of **1** and **2** in solution; the supported materials exhibited marked enhancements in stability and selectivity to (*Z*)-1-phenyl-1-propene.

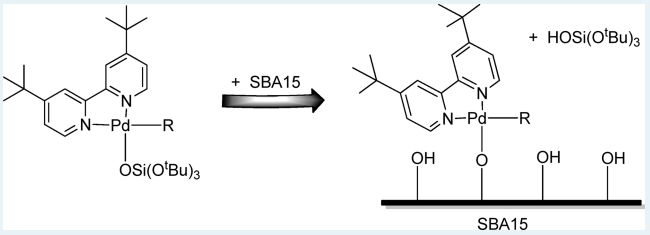

KEYWORDS: palladium-silica, thermolytic molecular precursor method, X-ray absorption, Pd(II) stability, 1-phenyl-1-propyne selective hydrogenation

INTRODUCTION

Heterogeneous catalysts often possess a wide variety of active sites, each with their own intrinsic reactivity. Thus, a major goal in catalysis research is the preparation of catalysts with well-defined and isolated sites, as such systems facilitate the investigation of structure−activity relationships in catalytic reactions and contribute to the rational design of new materials exhibiting superior performance and novel reactivity.[1−4] Supported palladium (Pd) centers are of particular interest because of the ability of Pd to effectively catalyze a wide variety of transformations, including selective hydrogenation, oxidation, and carbon−carbon bond formation.[5−7] The investigation of isolated, mononuclear Pd(II) sites on a solid support also offers the opportunity to compare stability and reactivity with related metallic nanoparticles and bulk metal. Nanoparticles may form during typical Pd^0-Pd(II) catalytic cycles, and the nanoparticles can play an important role in catalysis.[7−9] Furthermore, supporting the metal center onto a high surface area material can improve overall catalyst stability, efficiency, and reactivity, and provide opportunity for catalyst separation and reuse.[10−14]

The *thermolytic molecular precursor* (TMP) route has been used to introduce well-dispersed, isolated catalytic sites on surfaces.[10,12,13,15−18] The basic strategy involves the synthesis of a well-defined organometallic oxygen-rich molecular precursor that is incorporated into the solid support through a mild calcination procedure. The TMP method preserves the surface properties and allows for atomic level synthetic control, and presents an improvement over aqueous methods that result in metal aggregation.[16] Additionally, the TMP method provides an excellent spectroscopic model for the active site.[17,19,20] Previous applications of the method to late transition metals have yielded

Received: May 21, 2011
Revised: July 7, 2011
Published: July 18, 2011

highly disperse, isolated metal centers that share many of the same structural and spectroscopic characteristics as the corresponding molecular precursors.[10,12,13,15] For example, the molecular precursors (cod)Pt[OSi(O^{t}Bu)$_3$]$_2$ and Me$_3$Pt(tmeda)[OSi(O^{t}Bu)$_3$] were used to introduce isolated Pt(II) and Pt(IV) centers on silica, which were robust in inert atmosphere to similar decomposition temperatures as that of the precursors.[18] However, no Pd TMP-derived materials have been prepared and studied to date.

This report describes the synthesis and characterization of two tris(*tert*-butoxy)siloxy palladium(II) complexes of the form (4,4′-di-*tert*-butyl-2,2′-bipyridyl)Pd[OSi(O^{t}Bu)$_3$](R) (**1**, R = OSi(O^{t}Bu)$_3$ and **2**, R = CH$_3$). These compounds were covalently grafted onto the surface of mesoporous silica (SBA15) to generate supported Pd(II) centers. Additionally, they function as molecular models for the surface-bound Pd sites. The structures of the supported Pd centers were compared to those of **1** and **2** using Fourier-transform infrared (FTIR) spectroscopy, diffuse reflectance UV−vis (DRUV−vis) spectroscopy and X-ray absorption spectroscopy (XAS). The thermal stability of the supported Pd centers was examined, and the catalytic behavior of the **PdSBA15** materials in the semihydrogenation of 1-Phenyl-1-propyne was studied and compared to that of **1** and **2** in solution.

EXPERIMENTAL SECTION

General Procedures. All manipulations were conducted under a nitrogen atmosphere using standard Schlenk techniques or in a Vacuum Atmospheres drybox, unless otherwise noted. Dry, oxygen−free solvents were used throughout. Palladium(II) dichloride was purchased from Strem Chemicals, Inc. and Pressure Chemical Co., and used as received. Acetonitrile, 1-Phenyl-1-propyne, silver(I) oxide, and 4,4′-di-*tert*-butyl-2,2′-bipyridine (^{t}Bu$_2$-bpy) were purchased from Aldrich and used as received. Methyl iodide (Eastman Kodak) was obtained from the UC Berkeley Chemical Reuse Facility and used as received. Hydrogen (99.999%) was purchased from Praxair. Palladium Perkin-Elmer Pure ICP-OES calibration standard (matrix: 10% HCl) was diluted with 2% HNO$_3$ to form standard solutions for instrument calibration. The following were prepared according to literature procedures: dimethyl(*N*,*N*,*N*′,*N*′-tetramethylethanediamine)palladium(II),[21] HOSi(O^{t}Bu)$_3$,[22] KOSi(O^{t}Bu)$_3$,[23] and SBA15.[24]

Characterization. Benzene−d_6 was purified and dried by vacuum distillation from sodium/potassium alloy. For the characterization of compounds **1** and **2**, solution ^{1}H and ^{13}C NMR spectra were recorded at 400 and 100 MHz, respectively, using a Bruker AVQ-400 spectrometer. Solution 2D ^{1}H-^{29}Si HMQC NMR spectra were recorded using a Bruker AVB-400 spectrometer. For the catalytic studies, solution ^{1}H NMR spectra were recorded at 300 MHz using a Bruker AV-300 spectrometer. Chemical shifts for ^{1}H and ^{13}C NMR spectra were referenced internally to the residual solvent signal relative to tetramethylsilane. The single-crystal X-ray analyses of compounds **1** and **2** were carried out at the UC Berkeley CHEXRAY crystallographic facility.

Carbon, hydrogen, and nitrogen elemental analyses were performed by the College of Chemistry microanalytical laboratory at the University of California, Berkeley. Palladium elemental analyses were performed on a Perkin-Elmer Optima 3000 DV ICP-OES instrument. The samples were initially digested in 2 mL of concentrated HCl/HNO$_3$ (3:1) and 0.2 mL of 48% HF. The mixture was then heated to dryness, and the residue dissolved in hot, concentrated HCl (1 mL). Dilution to 25 mL with 2% HNO$_3$ yielded clear solutions for analysis. The Pd emission at 340.458 nm was measured, and the reported Pd content is the average of triplicates. In all cases the relative standard deviation was less than 4%.

Nitrogen adsorption isotherms were obtained using a Quantachrome Autosorb 1, and samples were outgassed at 120 °C for at least 20 h prior to measurement. The Brunauer−Emmet−Teller (BET) method[25] was used to determine surface area, and the Barrett−Joyner−Halenda (BJH) method[26] was used to obtain pore size distribution. Thermal analyses were performed on an EXSTAR TG/DTA6300 manufactured by Seiko Instruments Inc., with a heating rate of 10 °C min^{-1} under a flow of nitrogen or oxygen. The calcination of catalysts was performed using a Lindberg 1200 °C three-zone furnace with a heating rate of 10 °C min^{-1} under a flow of nitrogen. Powder X-ray diffraction (PXRD) experiments were performed on a Bruker D8 Discover X-ray diffractometer using Co Kα radiation. Transmission electron microscopy (TEM) was carried out on a Philips Tecnai 12 transmission electron microscope operating at 200 kV. Samples for TEM studies were prepared by depositing an acetone suspension of the material onto a carbon-coated copper grid obtained from Ted Pella, Inc. Infrared spectra were recorded on a Nicolet Nexus 6700 FTIR spectrometer with a liquid nitrogen cooled MCT-B detector. Measurements were made at 4.0 cm^{-1} resolution. The supported materials (20−25 mg) were pressed at 1000 psi for 30 s to produce 25 mm diameter self-supporting wafers. Diffuse reflectance UV−vis (DRUV−vis) spectra were recorded on a Varian Cary 4 UV−vis spectrometer with MgO as a reference.

X-ray absorption measurements were made on the insertion-device beamline (10-ID) of the Materials Research Collaborative Access Team (MRCAT) at the Advanced Photon Source (APS), Argonne National Laboratory (Argonne, IL). A cryogenically cooled double-crystal Si (111) monochromator was used in conjunction with an uncoated glass mirror to minimize the presence of harmonics. The monochromator scanned continuously during the measurements with data points integrated over 0.5 eV for 50 ms per data point. Measurements were made in transmission mode at the Pd *K* absorption edge (24.350 keV) with the ionization chambers optimized for maximum current with linear response (∼10^{10} photons detected per second) using a mixture of N$_2$ and He in the incident X-ray detector and a ∼20% Ar in N$_2$ in the transmission X-ray detector. A spectrum of a Pd foil was acquired simultaneously with each measurement for energy calibration. Phase shift and backscattering amplitudes were obtained from reference compounds (Pd(NH$_3$)$_4$(NO$_3$)$_2$ for Pd−N and Pd foil for Pd−Pd). Standard procedures based on WINXAS v.3.2 software[27] were used to extract the extended X-ray absorption fine structure (EXAFS) data. The coordination parameters were obtained by a least-squares fit in *k*- and *R*-space of the isolated multiple-shell, k^2-weighted Fourier transform data.

Catalyst samples (∼20−40 mg) were pressed into a cylindrical holder of ∼5 mm diameter in the absence of air using a glovebox purged with N$_2$. In the glovebox, the sample holder was loaded into a quartz tube (1 in. diameter) and fitted with Swagelok fittings containing Kapton windows for entry and exit of X-rays. X-ray absorption spectra of fresh samples were obtained in flowing He and/or H$_2$ (50 mL min^{-1}), while heat treated samples were exposed to temperatures ranging from room temperature to 300 °C. These samples were heated in He or 4% H$_2$/He mixture for a 1/2 h and then cooled to room

temperature in He before measurement of the X-ray absorption spectra. The XANES spectra of the thermally treated catalysts were fit using a linear combination of the unmodified supported catalyst and metallic Pd, that is, Pd foil. The EXAFS data of the Pd precursors were fit using the phase and amplitude functions of the references and the coordination geometry and bond distances provided by the single crystal data. The Debye−Waller factor (DWF) giving the best fit for the precursor was fixed in the fits of the supported and thermally treated catalysts.

(^{t}Bu$_2$-bpy)PdCl$_2$. The compound was prepared by modification of a literature procedure using $(CH_3CN)_2PdCl_2$, generated in situ, rather than $(PhCN)_2PdCl_2$.[28] The following reaction was performed in the air: $PdCl_2$ (1.064 g, 6 mmol) was refluxed in 150 mL of acetonitrile for 1 h to form a reddish-brown solution of $(CH_3CN)_2PdCl_2$. A 100 mL solution of 4,4′-di-*tert*-butyl-2,2′-bipyridine (1.609 g, 6 mmol) in acetonitrile was added in portions to the reaction flask, producing an immediate orange precipitate with each addition. The reaction mixture was refluxed for an additional 1 h and then cooled to room temperature and filtered with a Buchner funnel. The filter cake was washed sparingly with hexanes and allowed to air-dry. The resulting light-orange powder (2.41 g, 90.3%) was dissolved in dry dichloromethane and dried over Na_2SO_4 before introduction into the drybox. Anal. Calcd for $C_{18}H_{24}Cl_2N_2Pd$: C, 48.48; H, 5.39; N, 6.29. Found: C, 48.12; H, 5.47; N, 5.97. ^{1}H NMR (400 MHz, $CDCl_3$, 20 °C): δ 9.14 (d, 2H, J = 6.4 Hz), 7.91 (d, 2H, J = 1.6 Hz), 7.47 (dd, 2H), 1.43 (s, 18H, bpy-(CMe_3)$_2$).

(^{t}Bu$_2$-bpy)Pd[OSi(O^{t}Bu)$_3$]$_2$ (1). A 20 mL solution of KOSi(O^{t}Bu)$_3$ (0.678 g, 2.24 mmol) in dichloromethane was added dropwise over 5 min to a stirred solution of (^{t}Bu$_2$-bpy)$PdCl_2$ (0.500 g, 1.12 mmol) in 10 mL of dichloromethane. Stirring was continued at room temperature for 16 h before removal of the solvent in vacuo. The product was extracted from KCl with hexanes (5 × 20 mL). The cloudy extracts were allowed to settle overnight, resulting in sedimentation of a pale yellow powder. Filtration produced a clear yellow solution that was concentrated (60 mL) and cooled to −30 °C to afford **1** as translucent yellow-orange microcrystalline plates (0.343 g, 34.0%). Crystals suitable for X-ray structure analysis were grown via slow vapor diffusion of hexanes into a concentrated solution of **1** in toluene at −30 °C. Anal. Calcd for $C_{42}H_{78}N_2O_8PdSi_2$: C, 55.95; H, 8.72; N, 3.11. Found: C, 56.12; H, 8.73; N, 3.33. ^{1}H NMR (400 MHz, benzene-d_6, 20 °C): δ 9.51 (d, 2H, J = 6.0 Hz), 7.12 (d, 2H, J = 2.0 Hz), 6.95 (dd, 2H, J = 2.0, 6.4 Hz), 1.75 (s, 54H, OCMe_3), 0.89 (s, 18H, bpy-(CMe_3)$_2$). ^{13}C{^{1}H} NMR (400 MHz, benzene-d_6, 20 °C): δ 162.26, 155.76, 154.43, 122.78, 116.59, 71.75 (SiO-*C*-Me$_3$), 35.15 (bpy-*C*-Me$_3$), 32.94 (SiOC-*Me*$_3$), 30.17 (bpy-C*Me*$_3$). ^{29}Si NMR (99.4 MHz, benzene-d_6, 20 °C): δ −88.69 (s, O*Si*(O^{t}Bu)$_3$). IR (Nujol, KBr, cm^{-1}) 2964 s, 2897 s, 2856 s, 1617 m, 1547 w, 1463 s, 1415 w, 1379 m, 1359 m, 1241 m, 1219 m, 1196 m, 1066 s, 1042 s, 1020 s, 962 m, 845 w, 820 m, 723 w, 696 m, 637 w, 601 w, 546 w, 483 m. Mp 114−118 °C (dec).

(^{t}Bu$_2$-bpy)Pd(CH$_3$)$_2$. The compound was prepared by modification of a literature procedure for the corresponding 2,2′-bipyridine complex.[21] A 30 mL solution of 4,4′-di-*tert*-butyl-2,2′-bipyridine (1.17 g, 4.36 mmol) in benzene was added to a stirred solution of dimethyl(*N*,*N*,*N*′,*N*′-tetramethylethanediamine)-palladium(II) (1.07 g, 4.24 mmol) in 10 mL of benzene, whereupon the solution immediately changed from colorless to yellow. Stirring was continued for an additional 2 h before removal of the solvent in vacuo. The resulting residue was washed with 20 mL of diethyl ether followed by 20 mL of hexanes. After drying in vacuo a bright yellow powder was obtained (1.54 g, 89.5%). Anal. Calcd for $C_{20}H_{30}N_2Pd$: C, 59.33; H, 7.47; N, 6.92. Found: C, 59.65; H, 7.41; N, 7.01. ^{1}H NMR (400 MHz, benzene-d_6, 20 °C): δ 8.74 (d, 2H, J = 5.4 Hz), 7.56 (d, 2H, J = 1.8 Hz), 6.62 (dd, 2H), 1.36 (s, 6H, PdMe_2), 0.97 (s, 18H, bpy-(CMe_3)$_2$).

(^{t}Bu$_2$-bpy)Pd(CH$_3$)(I). The compound was prepared by modification of a literature procedure for the corresponding 2,2′-bipyridine complex.[29] Methyl iodide was added to a stirred suspension of (^{t}Bu$_2$-bpy)Pd(CH$_3$)$_2$ (0.250 g, 0.618 mmol) in 5 mL of benzene in one portion via a syringe (0.15 mL, 2.408 mmol). Gas evolution was immediate with subsequent formation of a clear yellow solution. After 15 min the reaction volume was reduced to about 2 mL and left to sit for 16 h at room temperature, during which the product crystallized as fine yellow needles (0.273 g, 85.6%). Anal. Calcd for $C_{19}H_{27}IN_2Pd$: C, 44.16; H, 5.27; N, 5.42. Found: C, 44.19; H, 5.01; N, 5.25. ^{1}H NMR (400 MHz, benzene-d_6, 20 °C): δ 9.58 (d, 1H, J = 5.6 Hz), 8.09 (d, 1H, J = 6.0 Hz), 7.62 (s, 1H), 7.56 (s, 1H), 6.60 (dd, 1H), 6.52 (dd, 1H), 1.54 (s, 3H, Pd*Me*), 1.03 (s, 9H, bpy-(CMe_3)$_2$), 1.00 (s, 9H, bpy-(CMe_3)$_2$).

(^{t}Bu$_2$-bpy)Pd(CH$_3$)[OSi(O^{t}Bu)$_3$] (2). Toluene (50 mL) was added to a flask containing (^{t}Bu$_2$-bpy)Pd(CH$_3$)(I) (0.630 g, 1.22 mmol), HOSi(O^{t}Bu)$_3$ (0.322 g, 1.22 mmol), and Ag_2O (0.331 g, 1.43 mmol). The contents were stirred in the dark at room temperature for 3 days. The resulting deep yellow solution was filtered, and the solvent was reduced to about 40 mL before cooling to −78 °C. The formed crystals were washed with cold hexanes (2 × 10 mL) and dried in vacuo to afford **2** as a bright yellow powder (0.567 g, 71.1%). Crystals suitable for X-ray structure analysis were grown via slow evaporation of a benzene solution at room temperature. Anal. Calcd for $C_{31}H_{54}N_2O_4PdSi$: C, 56.99; H, 8.33; N, 4.29. Found: C, 57.37; H, 8.30; N, 4.69. ^{1}H NMR (400 MHz, benzene-d_6, 20 °C): δ 9.91 (d, 1H, J = 5.2 Hz), 8.29 (d, 1H, J = 6.0 Hz), 7.38 (s, 1H), 7.32 (s, 1H), 7.28 (d, 1H, J = 5.2 Hz), 6.37 (d, 1H, J = 4.4 Hz), 1.85 (s, 27H, OCMe_3), 1.70 (s, 3H, Pd*Me*), 0.98 (s, 9H, bpy-(CMe_3)$_2$), 0.94 (s, 9H, bpy-(CMe_3)$_2$). ^{13}C{^{1}H} NMR (400 MHz, benzene-d_6, 20 °C): δ 161.89, 160.76, 157.68, 153.10, 150.97, 149.83, 123.30, 123.15, 118.42, 116.87, 71.24 (SiO-*C*-Me$_3$), 35.19 (bpy-*C*-Me$_3$), 35.06 (bpy-*C*-Me$_3$), 33.01 (SiOC-*Me*$_3$), 30.41 (bpy-C*Me*$_3$), 30.19 (bpy-C*Me*$_3$), 1.26 (Pd*Me*). ^{29}Si NMR (79.5 MHz, benzene-d_6, 20 °C): δ −79.63 (s, O*Si*(O^{t}Bu)$_3$). IR (Nujol, KBr, cm^{-1}) 2919 s, 2856 s, 1612 m, 1462 s, 1409 w, 1378 m, 1235 b, 1198 m, 1041 s, 1020 s, 838 w, 818 m, 722 w, 693 w, 484 b. Mp 50−52 °C (dec).

Preparation of Pd(1)SBA15. The SBA15 was dried at 120 °C in vacuo for 12 h and handled under a nitrogen atmosphere. A 0.50 g sample of SBA15 was suspended in hexanes (15 mL), and a hexanes solution (40 mL) of **1** (0.0865 g, 0.0959 mmol) was added at room temperature. The mixture was stirred at room temperature for 16 h and then filtered, and the resulting solid was washed with hexanes (3 × 25 mL). The colorless material was dried in vacuo for 2 h prior to storage in a drybox. The wt % of Pd was 1.89 wt %, as determined by ICP-OES.

Preparation of Pd(2)SBA15. The SBA15 was dried at 120 °C in vacuo for 12 h and was handled under a nitrogen atmosphere. A 1.00 g sample of SBA15 was suspended in benzene (60 mL), and a benzene solution (60 mL) of **2** (0.128 g, 0.1959 mmol) was added at room temperature. The mixture was stirred at room temperature for 16 h and then filtered, and the resulting solid was washed with hexanes (3 × 60 mL). The colorless material was

dried in vacuo for 2 h prior to storage in a drybox. The wt % of Pd was 1.90 wt %, as determined by ICP-OES.

Catalytic hydrogenation of 1-phenyl-1-propyne. A J. Young NMR tube was charged with the desired catalyst (ca. 0.005 g of either compound **1** or **2**, or ca. 0.010 g of either **Pd(1)SBA15** or **Pd(2)SBA15**), followed by 0.50 mL of benzene-d_6. 1-Phenyl-1-propyne (12.5 μL, 0.10 mmol) was added via syringe under positive N_2 flow. Ferrocene (0.010 g) was used as an internal standard. After three freeze−pump−thaw cycles, 1 atm of hydrogen (ca. 0.10 mmol) was added at room temperature. The reaction was heated in an oil bath at 50 °C. Substrate conversion and product assignment were determined via ^{1}H NMR spectroscopy. The turnover number (TON) was calculated as the ratio of the total moles of products formed to the moles of Pd. The selectivity was defined as the ratio of the moles of (*Z*)-1-Phenyl-1-propene to the total moles of products formed.

RESULTS AND DISCUSSION

Synthesis and Characterization of 1 and 2. The metathesis reaction of (^{t}Bu$_2$-bpy)PdCl$_2$ with 2 equiv of KOSi(O^{t}Bu)$_3$ in dichloromethane afforded the tris(*tert*-butoxy)siloxypalladium-(II) complex, (^{t}Bu$_2$-bpy)Pd[OSi(O^{t}Bu)$_3$]$_2$ (**1**; eq 1), in 34% yield as a translucent yellow-orange solid from hexanes.

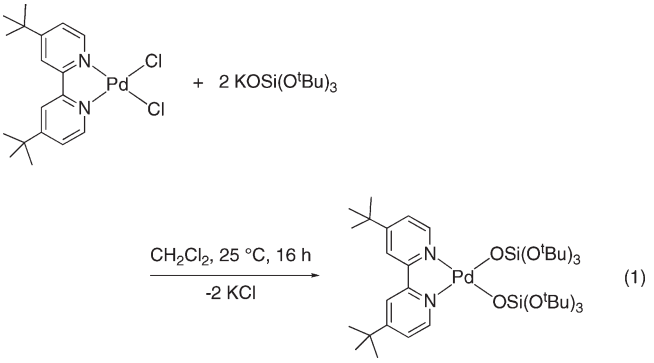

(1)

The major byproduct of the reaction was the monosubstituted palladium chloride complex, (^{t}Bu$_2$-bpy)Pd(Cl)[OSi(O^{t}Bu)$_3$], which was separated from the desired product by exploitation of its low solubility in hexanes relative to that of the bis-siloxide complex.

The room temperature ^{1}H NMR spectrum of **1** in benzene-d_6 exhibits a singlet at 1.75 ppm due to the −OSi(O^{t}Bu)$_3$ ligands. The *tert*-butyl protons of the coordinated ^{t}Bu$_2$-bpy ligand are seen as a singlet at 0.89 ppm. The aromatic ^{t}Bu$_2$-bpy protons resonate in the expected region of the spectrum at three different chemical shifts with two equivalent protons each and exhibit the appropriate splitting patterns. The ^{13}C and ^{29}Si NMR spectra are also consistent with the proposed structure. The ^{29}Si NMR spectrum contains a singlet at −88.69 ppm, slightly downfield from that of related platinum tris(*tert*-butoxy)siloxy complexes.[18] These multinuclear spectroscopic data provide strong evidence for a *cis* square planar geometry about the metal center, as expected from the chelating behavior of the bipyridine-based ligand.

The reaction of (^{t}Bu$_2$-bpy)Pd(CH$_3$)(I) with 1 equiv of HOSi(O^{t}Bu)$_3$ and 1.17 equiv of Ag$_2$O in toluene cleanly afforded the tris(*tert*-butoxy)siloxypalladium(II) complex (^{t}Bu$_2$-bpy)Pd(CH$_3$)[OSi(O^{t}Bu)$_3$] (**2**; eq 2), in 71% yield as a bright yellow solid. As a precaution, the flask was protected from light throughout the course of the reaction.

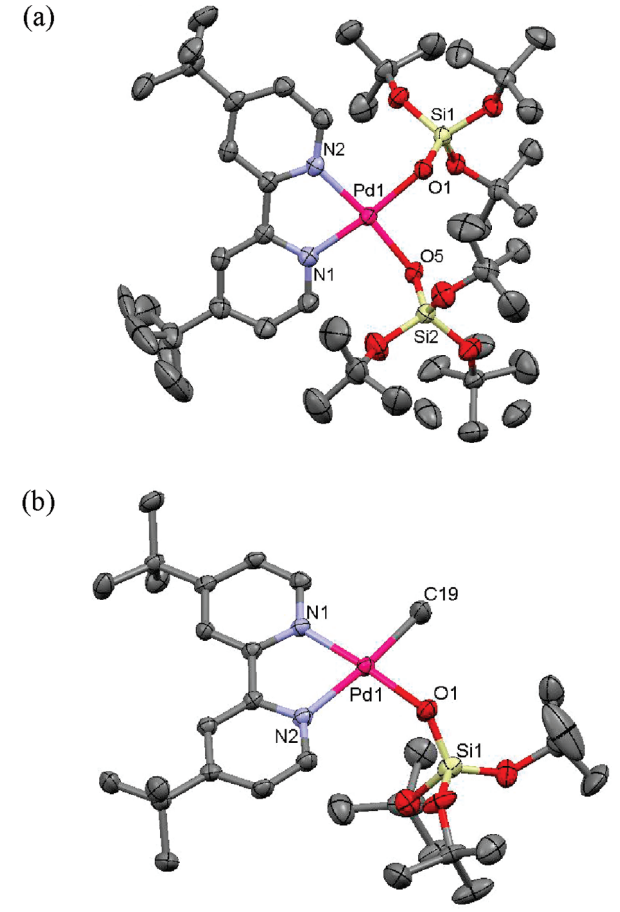

Figure 1. Molecular structures of (a) **1** and (b) **2** with thermal ellipsoids displayed at 50% probability. Hydrogens have been removed for clarity. Solvent molecules (benzene) have been removed for clarity in (b). Disorder was observed in the *tert*-butoxy group of **2**. Selected bond lengths and bond angles are found in Table 1.

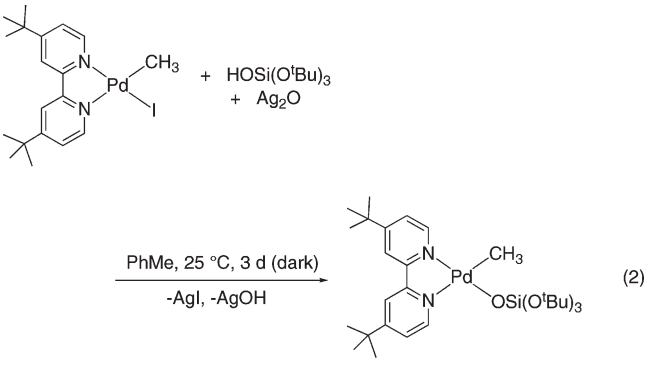

(2)

The room temperature ^{1}H NMR spectrum of **2** in benzene-d_6 exhibits a singlet at 1.85 ppm due to the equivalent *tert*-butoxy protons of the −OSi(O^{t}Bu)$_3$ ligand. The Pd−C*H*$_3$ resonance is observed as a singlet at 1.70 ppm. The resonances for the ^{t}Bu$_2$-bpy protons are in agreement with the proposed unsymmetrical structure of the complex. Specifically, the aromatic protons appear as six distinct peaks with appropriate splitting pattern.

dx.doi.org/10.1021/cs2002719 |*ACS Catal.* 2011, 1, 1166–1177

Table 1. Selected Bond Distances (Å) and Bond Angles (deg) for 1 and 2

distance		angle	
	(^{t}Bu$_2$-bpy)Pd[OSi(O^{t}Bu)$_3$]$_2$ (**1**)		
O(1)−Pd(1)	1.999(2)	N(1)−Pd(1)−N(2)	80.23(11)
O(5)−Pd(1)	1.993(2)	N(1)−Pd(1)−O(5)	93.40(10)
O(1)−Si(1)	1.597(2)	O(1)−Pd(1)−O(5)	92.15(9)
O(5)−Si(2)	1.590(2)	N(2)−Pd(1)−O(1)	94.40(10)
N(1)−Pd(1)	2.008(3)	Pd(1)−O(1)−Si(1)	118.36(12)
N(2)−Pd(1)	2.008(3)	Pd(1)−O(5)−Si(2)	124.48(12)
	(^{t}Bu$_2$-bpy)Pd(CH$_3$)[OSi(O^{t}Bu)$_3$] (**2**)		
O(1)−Pd(1)	2.003(2)	N(1)−Pd(1)−N(2)	79.00(9)
C(19)−Pd(1)	2.020(3)	N(1)−Pd(1)−C(19)	96.49(11)
O(1)−Si(1)	1.561(2)	O(1)−Pd(1)−C(19)	87.09(11)
N(1)−Pd(1)	2.022(2)	N(2)−Pd(1)−O(1)	97.53(9)
N(2)−Pd(1)	2.123(2)	Pd(1)−O(1)−Si(1)	136.67(14)

Furthermore, the *tert*-butyl protons of the coordinated ^{t}Bu$_2$-bpy ligand are seen as two singlets at 0.98 and 0.94 ppm. The ^{13}C and ^{29}Si NMR spectra are also consistent with the proposed structure. The ^{29}Si NMR shift at −79.63 ppm is slightly downfield from that of related platinum tris(*tert*-butoxy)siloxy complexes.[18] These NMR data provide strong evidence for the structure of the proposed complex.

Finally, the molecular structures of **1** and **2** were confirmed by single-crystal X-ray analysis and are consistent with the NMR data. The structure of **1** may be described as a slightly distorted *cis* square planar geometry about the Pd center (Figure 1a). A slightly distorted square planar geometry is also present in the structure of **2** (Figure 1b). Selected bond distances and angles are found in Table 1. In general, the Pd−N bond distances and the N−Pd−N bond angles for **1** and **2** are similar to those expected from reported Pd(II) complexes with a bidentate bipyridyl ligand.[30−33] In complex **2**, the Pd−N bond distance *trans* to the methyl group is elongated by about 0.1 Å compared to the other Pd−N bond distance, presumably from the *trans* influence of the methyl group. The Pd−OSi bond lengths in **1** are 1.999(2) and 1.993(2) Å and are within the range reported for alkoxo-palladium and aryloxo-palladium complexes (1.979−2.134 Å).[34,35] The Pd−OSi bond length of **2** (2.003(2) Å) also falls within this range. Similar compounds and corresponding Pd−O bond lengths are reported for the siloxypalladium complex [Pd(C$_6$F$_5$)(OSiPh$_3$)-(tmeda)] (1.986(3) Å)[36] and for arylpalladium silsesquioxanate compounds *trans*-[Pd{O$_{10}$Si$_7$(c-C$_5$H$_9$)$_7$(OH)$_2$}(C$_6$F$_5$)(PMe$_3$)$_2$] (2.098(3) Å)[35] and [Pd(C$_6$F$_5$){(c-C$_5$H$_9$)$_7$Si$_7$O$_{10}$(OH)$_2$}(tmeda)] (2.000(2) Å)[34] (tmeda = *N*,*N*,*N*′,*N*′-tetramethylethylenediamine). Finally, the Pd−O−Si bond angles in **1** are generally smaller than that in **2**, and this may be attributed to the increased steric bulk arising from the additional tris(*tert*-butoxy)siloxy ligand in **1**.

Solid-State Thermolytic Chemistry of 1 and 2. The thermal decomposition behavior of **1** and **2** was studied by thermogravimetric analysis (TGA) and differential scanning calorimetry (DSC). The TGA traces for **1** and **2** under an inert atmosphere (N$_2$) are given in Figure 2. Compound **1** exhibits a precipitous weight loss at about 195 °C corresponding to the onset of decomposition to form (^{t}Bu$_2$-bpy)Pd·SiO$_2$ (expected ceramic yield, 48.2%) followed by a gradual weight loss as the temperature is increased. The ceramic yield at 500 °C for **1** is 23.08%,

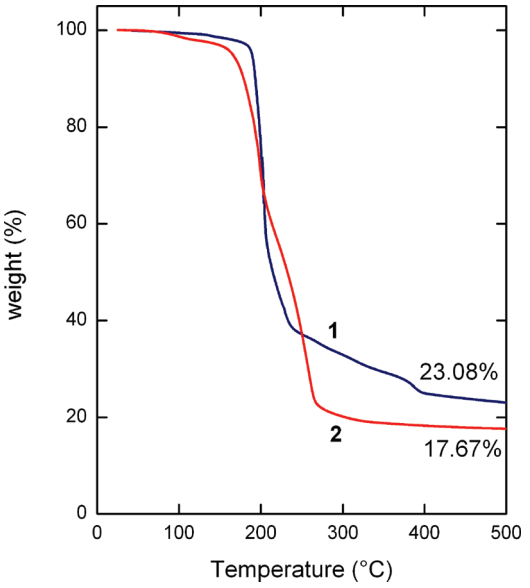

Figure 2. TGA traces for **1** and **2** under N$_2$ with a heating rate of 10 °C min^{-1}. The labels denote the final observed wt % at 500 °C.

which is similar to that expected for Pd·SiO$_2$ (18.5%) and suggests loss of the ligand past about 195 °C, presumably from volatilization or decomposition. The results were confirmed by decomposition of **1** under vacuum for 2 h at 250 °C and condensation of the volatile elimination products into an NMR tube containing benzene-d_6 and a ferrocene standard at −196 °C. HOSi(O^{t}Bu)$_3$, *tert*-butanol, isobutene and water were observed (1.1, 0.3, 0.2, and 0.2 equiv, respectively), while a black decomposition product containing uncoordinated ^{t}Bu$_2$-bpy remained. PXRD analysis of the solid, nonvolatile products indicated the formation of Pd^0. Decomposition of **1** was rapid and exothermic under an O$_2$ atmosphere, presumably from the Pd-catalyzed combustion of organic byproducts, and resulted in the formation of a light brown solid in a ceramic yield of 14.30%, which is similar to that expected for PdO (13.6%) (Supporting Information, Figure S1). The DSC analysis of **1** under N$_2$ displays an endothermic transition at about 195 °C associated with the beginning of decomposition. An additional endothermic transition at about 117 °C is attributed to the melting point, which was confirmed with a Mel-Temp apparatus.

For compound **2**, decomposition begins at about 195 °C and appears to proceed directly to Pd black. The ceramic yield at 500 °C for **2** is 17.67%, which similar to that expected for Pd^0 (16.3%). The results were confirmed by decomposing **2** under vacuum for 2 h at 250 °C and condensing the volatile elimination products into an NMR tube containing benzene-d_6 and a ferrocene standard at −196 °C. Minor amounts (<0.1 equiv) of *tert*-butanol, isobutene, water, and methane were observed, along with 0.4 equiv of HOSi(O^{t}Bu)$_3$. A black decomposition product containing uncoordinated ^{t}Bu$_2$-bpy remained. PXRD analysis of the solid, nonvolatile products indicated the formation of Pd^0. Decomposition of **2** was rapid and exothermic under an O$_2$ atmosphere, presumably from the Pd-catalyzed combustion of organic byproducts, and resulted in the formation of a light brown solid in a ceramic yield of 19.95%, which is similar to that expected for PdO (18.7%) (Supporting Information, Figure S1). The thermolytic behavior of **1** and **2** is similar to that observed for other late transition-metal (alkoxy)siloxy complexes, which result in

dx.doi.org/10.1021/cs2002719 |*ACS Catal.* 2011, 1, 1166–1177

Table 2. Nitrogen Porosimetry and Palladium Loading Data for the Pd-SBA15 Materials

material	Pd content (wt %) ICP-OES[d]	Pd coverage (Pd nm^{-2})	S_{BET} (m^2 g^{-1})	r_{pore} (nm)	$V_{pore,avg}$ (cc g^{-1})
SBA-15[a]			666	2.8	0.685
Pd(1)SBA15[b]	1.89	0.16	458	2.8	0.500
Pd(2)SBA15[c]	1.90	0.16	467	2.8	0.504

[a] 2.3(1) OH/nm^2 by titration with $Mg(benzyl)_2(THF)_2$. [b] Maximum loading experimentally determined to be 5.0 wt %Pd (0.42 Pd nm^{-2}). [c] Maximum loading experimentally determined to be 5.1 wt %Pd (0.43 Pd nm^{-2}). [d] Average value of triplicates with relative standard deviations <4% in all cases.

Scheme 1. Grafting Chemistry of 1 (R = OSi(O^{t}Bu)$_3$) and 2 (R = CH$_3$) onto the Surface of SBA15

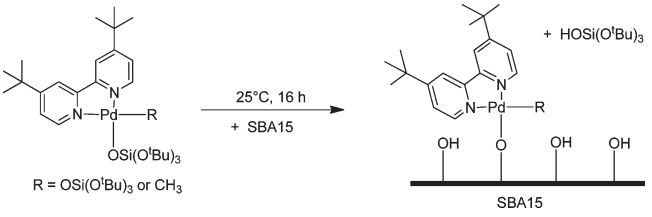

the elimination of HOSi(O^{t}Bu)$_3$ and formation of reduced metal, presumably via M-O bond homolysis.[10,18,20,37]

Preparation of Pd(1)SBA15 and Pd(2)SBA15. The mesoporous silica SBA15 was prepared according to a literature procedure and characterized by PXRD and N_2 porosimetry prior to catalyst preparation. The surface area, pore radius, and pore volume data for the unmodified SBA15 are presented in Table 2. The adsorption−desorption data for the unmodified SBA15 is shown in Supporting Information, Figure S2A and corresponds to a type IV isotherm, as expected of mesoporous SBA15 materials. The PXRD pattern displayed the characteristic small-angle (100) reflection of the mesostructured architecture (Supporting Information, Figure S2B). The hydroxyl group surface coverage of the SBA15 was determined to be 2.3 ± 0.1 OH nm^{-2} via titration with $Mg(CH_2C_6H_5)_2 \cdot 2THF$ and quantification of the evolved toluene by ^{1}H NMR spectroscopy.[17]

Precursors **1** and **2** were grafted onto the silica surface by addition of a solution of the precursor to a stirred suspension of SBA15 in the same solvent (benzene) under N_2 at room temperature. The use of low concentrations of **1** and **2** ensured low wt % Pd-silica materials (ca. 2.0 wt %) with a high spatial dispersity of Pd centers on the surface (ca. 0.20 Pd nm^{-2}). After 16 h the solid was filtered, washed with hexanes, and dried in vacuo at room temperature to quantitatively yield the colorless materials **Pd(1)SBA15** and **Pd(2)SBA15**. The wt % of Pd was determined to be 1.89 and 1.90 wt %, respectively, by ICP-OES. These values correspond to 0.16 Pd nm^{-2} for both **Pd(1)SBA15** and **Pd(2)SBA15**.

Solution ^{1}H NMR spectroscopy was used to monitor the reactions of **1** and **2** with SBA15. Protonolysis of the Pd−OSi bond by the surface Si−OH groups should result in the elimination of HOSi(O^{t}Bu)$_3$. Compound **2** may also react via the Pd−CH$_3$ bond to eliminate CH_4. The reaction between excess **1** and SBA15 in benzene-d_6 at room temperature generated an average of 0.94 equiv of the silanol per equiv of reacted **1** (based on a ferrocene internal standard) (Scheme 1, R = OSi(O^{t}Bu)$_3$). The amount of **1** consumed corresponds to a maximum Pd loading of 5.0 wt % (0.42 Pd nm^{-2}). Similarly, the reaction between excess

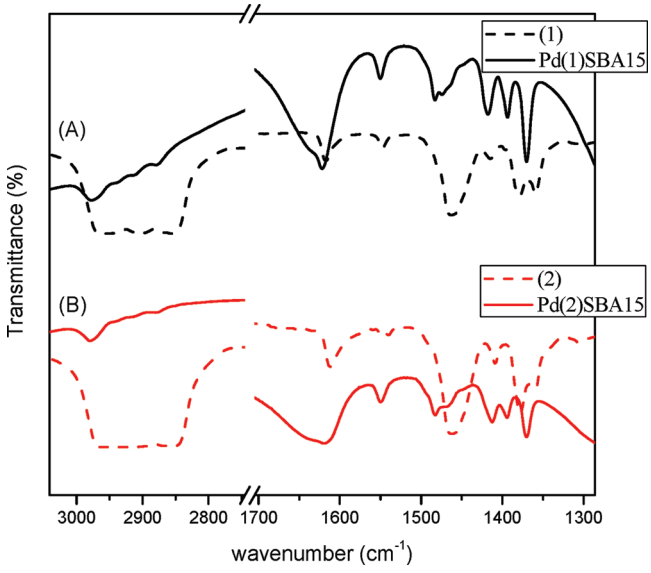

Figure 3. Transmission FTIR spectra for (A) **1** and **Pd(1)SBA15** and (B) **2** and **Pd(2)SBA15**. Spectra are offset for clarity.

2 and SBA15 in benzene-d_6 at room temperature generated an average of 0.97 equiv of the silanol per equiv of reacted **2** (based on a ferrocene internal standard) (Scheme 1, R = CH$_3$). Furthermore, no CH_4 was observed by ^{1}H NMR spectroscopy. The amount of **2** consumed corresponds to a maximum Pd loading of 5.1 wt % (0.43 Pd nm^{-2}).

Characterization of Pd(1)SBA15 and Pd(2)SBA15. Nitrogen porosimetry was used to evaluate the surface area and pore structure of the new materials. The adsorption−desorption data for each material correspond to type IV isotherms, which are characteristic of mesoporous SBA15-type materials. The surface area, pore radius, and pore volume data for the materials are presented in Table 2. The narrow pore size distribution of SBA15 was preserved upon grafting of **1** and **2**, and as expected the Pd-containing materials have reduced surface area and average pore volume relative to SBA15.

The precursor complexes were designed with -OSi(O^{t}Bu)$_3$ ligands to mimic a silica environment, and thus **1** and **2** represent good spectroscopic models of mononuclear Pd centers supported on silica. The surface structures for the silica-supported Pd materials were compared with the molecular precursors by Fourier-transform infrared (FTIR) spectroscopy. The FTIR spectrum for the surface-supported Pd materials was difficult to obtain because of the silica background from SBA15. However, several bands corresponding to the ^{t}Bu$_2$-bpy ligand were identified (Figure 3, Supporting Information, Table S2) that confirm the coordination of the

dx.doi.org/10.1021/cs2002719 |ACS Catal. 2011, 1, 1166–1177

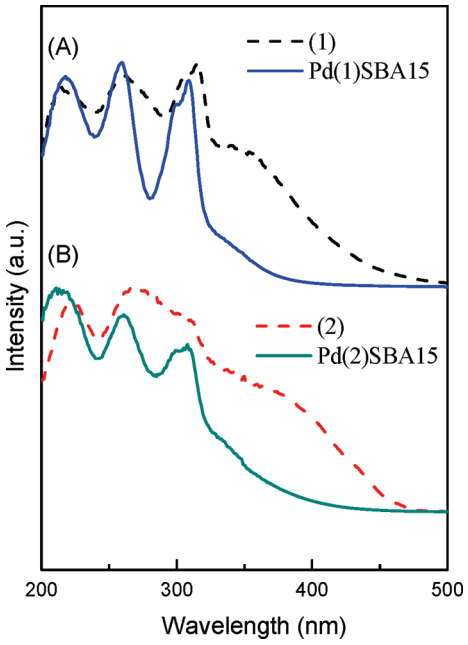

Figure 4. DRUV−vis spectra for: (A) **1** and **Pd(1)SBA15**; and (B) **2** and **Pd(2)SBA15**, offset for clarity. The spectra were normalized to the maximum absorbance. MgO was used as a reference.

ligand to the metal center. Analogous peaks were observed in the FTIR spectra of the corresponding molecular precursors (Figure 3, Supporting Information, Table S2), which suggests that the (^{t}Bu$_2$-bpy)Pd core is intact for the surface Pd species and that the geometry of the supported Pd species is similar to that observed in the molecular precursors. The surface structures were further probed by UV−vis spectroscopy. The DRUV−vis spectra of **1**, **2**, **Pd(1)SBA15**, and **Pd(2)SBA15** are displayed in Figure 4. The values of the absorption maxima are also shown in Supporting Information, Table S2. Based on comparisons with the DRUV−vis spectra of the dichloro complex of **1**, the iodomethyl complex of **2**, bis(acetonitrile)PdCl$_2$, and the uncoordinated ^{t}Bu$_2$-bpy ligand, the strong high energy absorptions below 320 nm may tentatively be assigned as $\pi \rightarrow \pi^*$ transitions for coordinated ^{t}Bu$_2$-bpy, while the weak, broad low energy absorption centered around 350 nm may tentatively be assigned as a charge transfer band between Pd(II) and ^{t}Bu$_2$-bpy. The similarities in the maxima positions and shape of absorbance bands in the spectra of **1**, **2**, **Pd(1)SBA15**, and **Pd(2)SBA15** suggest the relatively small electronic effect on the surface structure upon changing the ligand from OSi(O^tBu)$_3$ to CH_3, and that the coordination environment about the metal centers of **1** and **2** is preserved upon grafting.

XAS of both **1** and **Pd(1)SBA15** were examined in the solid state to determine whether **1** remained intact upon grafting to the SBA15 silica surface (Scheme 1). Figures 5A and B are a comparison between the XANES and EXAFS region of the X-ray absorption spectra for the precursor (diluted in boron nitride powder) and the **Pd(1)SBA15** catalyst. It is apparent from the XANES region that the Pd centers in **1** are divalent and remain so after grafting to the silica surface. Similarly, there is no apparent change in the extended region of the spectrum which gives an indication of the number and identity of nearest neighbors. Therefore, XANES and EXAFS demonstrate that the oxidation state remains 2+, and Scheme 1 represents a plausible mechanism for grafting. There does not appear to be any significant differences in the fits. The coordination number is ∼4 for both the precursor **1** and the corresponding, grafted catalyst. It must be noted that there was no attempt to differentiate between the Pd−O and Pd−N coordination because of the similar phase shift and backscattering amplitude of the light atoms (O and N). The grafting of Pt(II) and Pt(IV)-siloxy complexes to silica with conservation of the original precursor oxidation state and coordination environment was reported previously.[18]

Thermolytic Chemistry of Supported Pd Centers. The stability of the silica-supported Pd centers toward decomposition was initially investigated by TGA. The TGA traces for **Pd(1)SBA15** and **Pd(2)SBA15** under N_2 are shown together in Figure 6. The initial weight loss below 100 °C is associated with water that physisorbed to the silica surface upon transfer of the sample from the drybox to the instrument, and does not represent decomposition of the Pd center. A similar initial weight loss was observed for unmodified SBA15. Thus, a reasonable estimate of the water content was determined from the initial weight loss below 120 °C, represented by the dashed line in Figure 6. The initial weight losses were 5.24% and 3.92% for **Pd(1)SBA15** and **Pd(2)SBA15**, respectively. The onset of weight loss for **Pd(1)SBA15** occurs at about 150 °C followed by a more precipitous loss at about 300 °C, resulting in a total weight loss of 10.45% from 120 to 500 °C (8.07% after subtraction of the weight loss associated with unmodified SBA15). The observed weight loss corresponds to a Pd loading of 1.49%, which is in close agreement with the results of ICP-OES. The loss is attributed to decomposition of the supported (^{t}Bu$_2$-bpy)PdOSi(O^tBu)$_3$ species based on the similarity of onset temperatures for precursor **1** and **Pd(1)SBA15**. However, the more gradual weight loss exhibited by the supported material suggests a less rapid decomposition to Pd metal in comparison to the precursor. For **Pd(2)SBA15**, a steady, gradual weight loss was observed beginning at about 150 °C followed by a more substantial loss at about 350 °C, which resulted in a total weight loss of 6.82% from 120 to 500 °C (6.20% after subtraction of the weight loss associated with unmodified SBA15). The observed weight loss corresponds to a Pd loading of 2.33%, which is in close agreement with the results of ICP-OES. The loss is attributed to decomposition of the supported (^{t}Bu$_2$-bpy)Pd(CH_3) species based on the similarity of onset temperatures for precursor **2** and **Pd(2)SBA15**. Similar to what was found for **Pd(1)SBA15**, the more gradual weight loss exhibited by **Pd(2)SBA15** suggests a less rapid decomposition to Pd metal in comparison to precursor **2**. Further weight loss from 500 °C onward is attributed to dehydroxylation of the silica support and amounts to about 2% for both materials.[18] The supported Pd centers were in general more thermally stable than their molecular counterparts.

In situ FTIR spectroscopy was also used to probe the thermal stability of the Pd centers. Under inert gas flow (He, 25 mL min^{-1}), **Pd(2)SBA15** was heated to 180 °C and held for 2 h. No changes in the characteristic peaks were detected during this time. However, a slight decrease in peak intensity was observed beginning at about 100 °C, which became more pronounced after 2 h of heating at 180 °C. Thus, the FTIR spectra are consistent with the TGA data, and indicate that the supported Pd centers are robust to temperatures near the decomposition temperature of the precursors.

To confirm the formation of Pd metal as a decomposition product, PXRD and TEM were employed. Samples of **Pd(2)SBA15** were heated under N_2 for 2 h at 200, 300, 400, and 500 °C to yield

dx.doi.org/10.1021/cs2002719 |*ACS Catal.* 2011, 1, 1166–1177

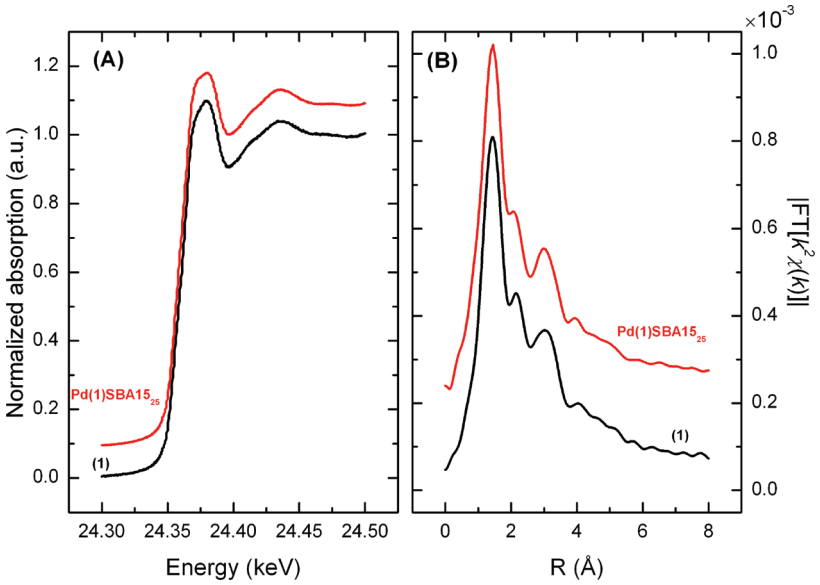

Figure 5. (A) XANES and (B) extended (EXAFS) region of Pd K-edge for (**1**) and **Pd(1)SBA15** at room temperature. The spectra for the solid-state precursor and room-temperature grafted species are nearly identical. Upon grafting there is no significant change in the Pd precursor. Supporting Information, Table S4 summarizes the results of the EXAFS fits. Analysis of the XANES spectra demonstrates the Pd centers present in the precursor and room-temperature grafted sample are Pd^{2+}.

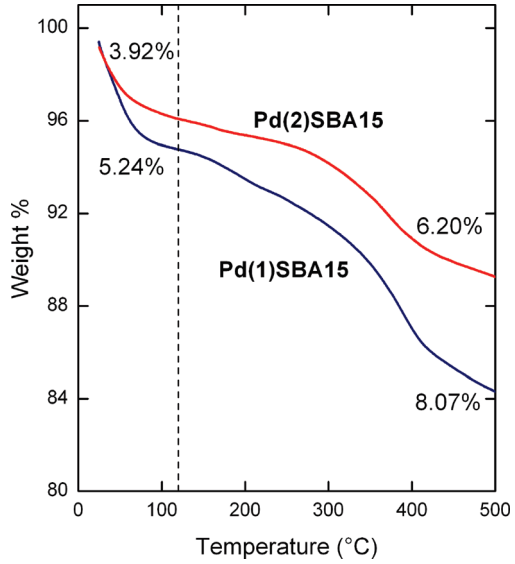

Figure 6. TGA traces for **Pd(1)SBA15** and **Pd(2)SBA15** under N_2 with a heating rate of 10 °C min^{-1}. The dashed line marks 120 °C, and the labels denote the observed wt % loss from either 25 to 120 °C (left of dashed line) or 120 to 500 °C (right of dashed line). The wt % loss has been corrected with a background subtraction of the blank SBA15 contribution.

the corresponding **Pd(2)SBA15**$_x$ materials, where x denotes the treatment temperature. The material changed color from white to dark gray during the heat treatment. The PXRD patterns for **Pd(2)SBA15**, **Pd(2)SBA15**$_{300}$, **Pd(2)SBA15**$_{400}$, and **Pd(2)SBA15**$_{500}$ are shown in Supporting Information, Figure S5. Diffraction peaks corresponding to metallic Pd^0 become apparent at 400 °C and appear to slightly sharpen at 500 °C.[38] The significantly broad, low intensity of the peaks suggest the formation

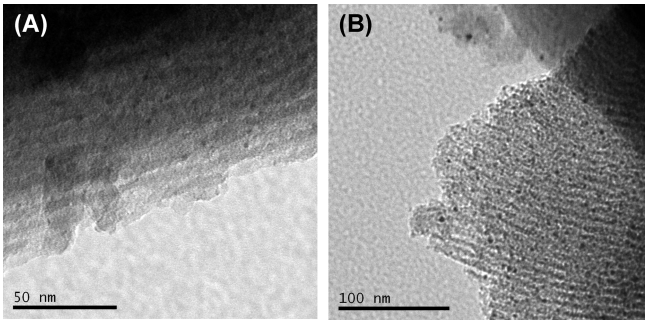

Figure 7. Representative TEM images of (a) **Pd(2)SBA15**$_{300}$ and (b) **Pd(2)SBA15**$_{500}$.

of highly disperse, small clusters and nanoparticles that are around the detection limit of the instrument (<3 nm diameter). Indeed, TEM imaging of **Pd(2)SBA15**$_{500}$ revealed isolated Pd nanoparticles with an average diameter of 2.3(8) nm (Figure 7b). TEM imaging of **Pd(2)SBA15**$_{300}$ revealed slightly smaller Pd nanoparticles with an average diameter of 1.6(7) nm, but only a small number of particles were confidently resolved through the thick walls of SBA15 (Figure 7a). These data suggest that the thermal decomposition of the supported Pd centers behaves analogously to that of the precursors, resulting in the formation of Pd metal.

For lower decomposition temperatures, the supported centers may form even smaller particles. PXRD is limited by peak broadening and the thick, amorphous walls of SBA15 may hinder the resolution of small particles by transmission electron microscopy (TEM).[18] Thus, XAS was employed to gain further insight into the nature of the metal center. Preliminary fits of the EXAFS spectra for **Pd(1)SBA15** suggest that as the temperature increases, the Pd−C, Pd−O, and Pd−N bonds dissociate, and Pd aggregates to form Pd−Pd bonds.

dx.doi.org/10.1021/cs2002719 |*ACS Catal.* 2011, 1, 1166–1177

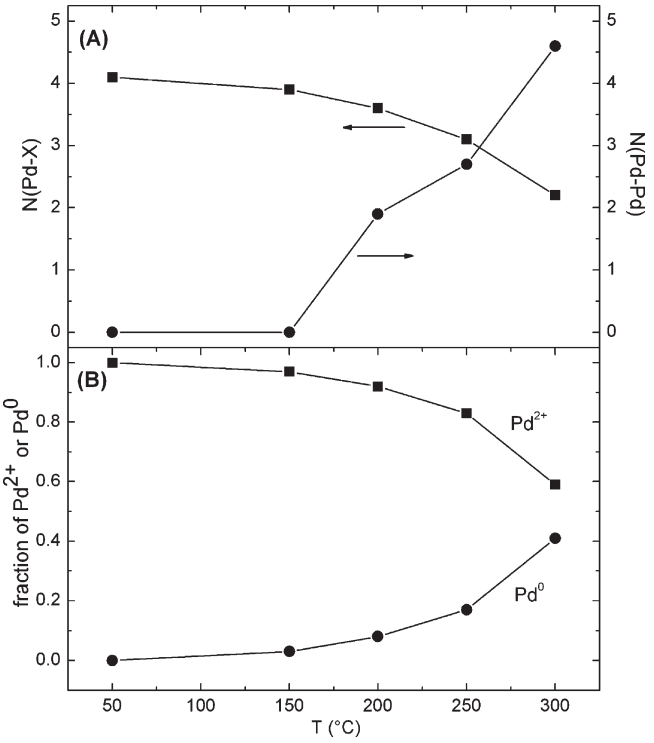

Figure 8. (A) Change in the Pd−X and Pt−Pt coordination number and (B) fraction of Pd^{2+}/Pd^0 as a function of temperature in He for **Pd(1)SBA15**. All XANES and EXAFS analyses were performed at room temperature after heating for a 1/2 h at the temperature specified on the *x*-axis. The corresponding EXAFS and XANES spectra for each of the data points in this figure are provided in the Supporting Information.

The precursor **1** and the **Pd(1)SBA15** sample were subjected to heat treatment under both He and hydrogen atmospheres at temperatures up to 300 °C. The precursor was examined as a function of temperature in He. A summary of the temperature dependent XANES and EXAFS data are included in Supporting Information, Tables S3 and S4. At 50 °C, the extended region is very similar to that of the room temperature spectra. At the highest temperature examined, the coordination number of Pd−Pd scatterers for the precursor **1** is 8.6. For the supported catalyst, the number of Pd−X (X = N or O) bonds remains near four at temperatures between 150 and 200 °C. By 200 °C, there is evidence for Pd−Pd scatterers, which increases with increasing temperature. These results are in qualitative agreement with TGA results for **1** in N_2 (Figure 2), which demonstrate a precipitous weight loss right before 200 °C. At the highest temperature examined (300 °C), the Pd−Pd coordination number is 4.6. Supporting Information, Figure S4 is the stacked EXAFS spectra of the **Pd(1)SBA15** catalyst after treatment at the specified temperature for 30 min in He followed by cooling to room temperature (temperature at which XAS data was collected). The near-edge spectra of the **Pd(1)SBA15** material was also examined as a function of temperature. The spectral data is included in Supporting Information, Figure S3, and the results are summarized in Supporting Information, Table S3. After exposure to He at 200 °C, analysis of the XANES region demonstrates that 92% of the Pd is in the +2 oxidation state, while at 300 °C in He, the catalyst is still 60% Pd^{2+}. Figure 8 summarizes the EXAFS and XANES results for the **Pd(1)SBA15** exposed to He at various temperatures.

In addition to examining the thermal stability of the supported **Pd(1)SBA15** material in He, we also examined structural changes with temperature in a H_2 environment. In hydrogen, changes to the XANES region were observed at 150 °C. At a temperature of 300 °C, analysis of the XANES region demonstrated that 70% of Pd^{2+} had been reduced to Pd(0). Supporting Information, Figure S3 and Table S3 demonstrates the influence of reduction temperature on the proportion of $Pd^{2+}/Pd(0)$ present in the catalyst after treatment in He or H_2 at temperatures up to 300 °C. These results demonstrate that these Pd^{2+} precursors are rather resilient to reduction. All spectra were taken in He at room temperature after purging the **Pd(1)SBA15** material in He at the same temperature used for the H_2 treatment. It is well-known that adsorbed hydrogen on late transition metal nanoparticles leads to an observable lengthening of the M−M bond. On Pd nanoparticles, hydrogen can be absorbed into the bulk to form a palladium hydride[39] leading to an expansion of the Pd−Pd bond length by 2−7% relative to the value in an inert atmosphere.[40,41] A recent study of the solubility of H_2 and subsequent hydride formation in small Pd nanoparticles supported on SiO_2 and Al_2O_3 involved Pd K- and L_{III}-edge XAS.[42] Hydride formation was detected directly at the L_{III}-edge, and it was observed that the ratio of hydrogen on the surface versus bulk hydrogen increased with decreasing particle size. It was also apparent that smaller particles dissolved less hydrogen.

From the EXAFS region after reduction of **Pd(1)SBA15** at elevated temperatures under hydrogen, the Pd−Pd coordination numbers were smaller than those observed in He at the same pretreatment temperature (Supporting Information, Table S4), and the Pd−Pd bond lengths are consistent with the absence of any hydride phase. This phase cannot be supported on the nanoparticles formed in this study because of their extremely small size. The largest particles were formed at the highest temperature (300 °C), and subsequently purged at that same temperature in He. This temperature is significantly greater than the temperature (100 °C) utilized by Boudart and co-workers to minimize the formation of the β-PdH phase during H_2-O_2 titration measurements of Pd surface areas.[43] All **Pd(1)SBA15** catalysts were purged with He at the temperature of reduction for 1/2 h; at these temperatures in the absence of gas-phase hydrogen, the hydride is unstable. We believe that the particles formed in this work upon exposure to hydrogen may be too small to accommodate hydrogen in their lattice, although future experiments at the Pd L_{III} edge which has a characteristic signature for hydride formation could confirm this assumption. The full EXAFS spectra for **Pd(1)SBA15** are provided as a stacked plot in the Supporting Information, Figure S4.

It is interesting to compare the coordination numbers (Supporting Information, Table S4) for the He- and H_2-treated **Pd(1)SBA15** samples. The Pd−Pd coordination number in He at 300 °C is almost twice that of the coordination number in H_2 at 300 °C (8.6 versus 4.4). It appears that the catalyst is more resilient to particle nucleation and growth under H_2, as compared to He. In He, it appears that the coordination number levels off to ~8.5, which corresponds to a particle size of 3.5 nm.[44]

Catalytic Alkyne Hydrogenation. Palladium catalysts are commonly used in selective hydrogenations. A prominent example is the commercially available Lindlar catalyst (Pd supported on $CaCO_3$ and poisoned with Pb and quinoline).[45] The semihydrogenation of alkynes to alkenes is a particularly facile reaction that proceeds in the presence of other functional groups.[46] The mechanism put forth by Horiuti−Polanyi in 1934 for the

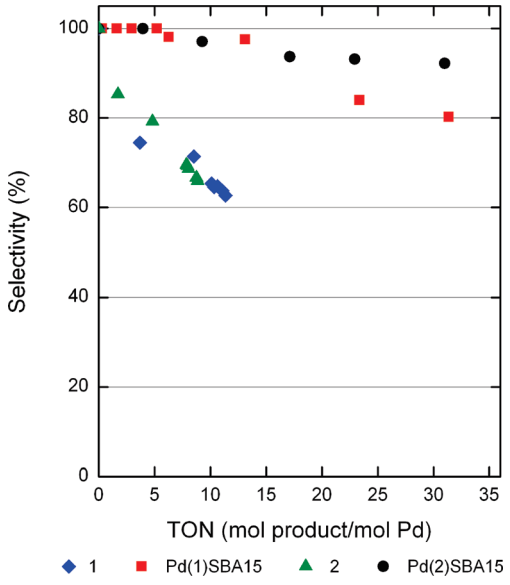

Figure 9. Selectivity versus turnover number (TON, mol products (mol Pd)$^{-1}$) for the hydrogenation of 1-phenyl-1-propyne, as catalyzed by either (blue diamonds) **1**, (black circles) **2**, (red squares) **Pd(1)SBA15** or (green triangles) **Pd(2)SBA15**. Selectivity is defined as the ratio of the moles of (*Z*)-1-phenyl-1-propene produced to the total moles of products formed. Conversion and product assignment were determined via ^{1}H NMR spectroscopy. Reaction conditions: 0.5 mL of C_6D_6, 50 °C and 1 atm H_2 in a sealed J-Young NMR tube.

heterogeneous hydrogenation of ethene has been used as a framework to understand the selectivity of the reaction for production of *cis*-alkenes, as well as the formation of alkanes and isomerization products.[45,47] Improved selectivity and activity may be obtained through the use of various supports, and thus it is of interest to compare the performance of catalysts under homogeneous and heterogeneous conditions.[48−51]

The performance of the supported Pd centers in the catalytic hydrogenation of 1-phenyl-1-propyne to (*Z*)-1-phenyl-1-propene was studied and compared to that of the precursors. As expected, unmodified SBA15 was completely inactive and thus any activity can be solely attributed to the presence of Pd. Additionally, filtration of the reaction mixture after about 25% substrate conversion and subjecting the filtrate to fresh reactants produced no further activity, providing strong evidence against leaching of Pd from SBA15. Figure 9 describes the selectivity for formation of (*Z*)-1-phenyl-1-propene versus turnover number (TON, mol products (mol Pd)$^{-1}$), as catalyzed by **1**, **2**, **Pd(1)SBA15** and **Pd(2)SBA15**. Besides (*Z*)-1-phenyl-1-propene, the other products observed were propylbenzene and minor amounts of (*E*)-1-phenyl-1-propene. The results demonstrate a rapid decline in selectivity to about 65% over an increase in TON to about 11 (2 h) for complex **1**. Similarly, in the case of **2**, selectivity fell to about 69% over an increase in TON to about 8 (2 h). For both complexes **1** and **2**, the reaction occurred with decomposition (vide infra) followed by a complete loss of activity. In contrast, the supported Pd centers displayed superior selectivity and stability, albeit at a slower rate. **Pd(1)SBA15** exhibited a high selectivity (>97%) over an increase in TON to about 13 that eventually dropped to about 80% at a TON of about 31 (31 h). **Pd(2)SBA15** behaved similarly to **Pd(1)SBA15** at low TON, but maintained an even higher selectivity (>92%) over an increase in TON to about 31 (5 h).

Thus, under the same conditions the supported Pd centers were significantly more selective than the homogeneous precursors and maintained a high selectivity over the course of the reaction. This may be due in part to the enhanced stability against particle agglomeration and preservation of the supported isolated Pd center. Similar results have been found in the semihydrogenation of 1-heptyne, as catalyzed by $PdCl_2L_2$ (L = $NH_2(CH_2)_{12}CH_3$ or $NH_2(CH_2)_5CH_3$) under homogeneous versus heterogeneous conditions;[49] and in the partial hydrogenation of 2-butyne-1,4-diol, as catalyzed by Pd nanoparticles supported in the micelle core of poly(ethylene oxide)-block-poly-2-vinylpyridine versus unsupported nanoparticles.[50] Catalysis with both complexes **1** and **2** occurred with noticeable decomposition (ca. 80% for **1** and ca. 60% for **2**) to form $HOSi(O^tBu)_3$, uncoordinated $^tBu_2$-bpy and a black precipitate, which is presumably Pd black. In the case of **Pd(1)SBA15**, about 1 equiv of $HOSi(O^tBu)_3$ with respect to Pd was observed, as expected from the proposed surface structure of the metal site (Scheme 1). No ligand hydrogenation products were observed for **Pd(2)SBA15**, but the formation of CH_4 in an undetectable concentration is a possibility. Additionally, for both **Pd(1)SBA15** and **Pd(2)SBA15**, a color change from white to pale gray was observed following catalytic testing, similar to that observed upon heat treatment of the **Pd(2)SBA15** material (vide supra). The results suggest that the supported Pd centers may decompose to form catalytically active Pd clusters or Pd^0 sites.

To further investigate this phenomenon, the catalytic activities of recycled **Pd(2)SBA15** and the heat treated **Pd(2)SBA15$_x$** materials were compared. Supporting Information, Figure S6 describes the variation in the initial observed turnover frequencies (TOF, h^{-1}) and overall % selectivity with the temperature of heat treatment. The TOF was found from a linear fit of the initial TON versus time data. A clear trend of increasing initial TOF with higher treatment temperatures was observed. **Pd(2)SBA15$_{500}$** exhibited a near 30-fold increase in TOF compared to that of the as-prepared material; however, this also corresponded to a drop in overall selectivity from over 90% to less than 60%. Furthermore, **Pd(2)SBA15** was recycled by filtration of the spent reaction mixture at a TON of about 50 (21 h), followed by washing the isolated solids with approximately 5 mL of benzene and 5 mL of hexanes. The obtained pale gray solids were dried under vacuum and subjected to fresh reactants under the same hydrogenation conditions described above. The initial TOF of the recycled **Pd(2)SBA15** was about twice that of the as-prepared material (2.26 vs 1.16 h^{-1}) and corresponded to a slight decrease in selectivity of about 5%. Based on the thermolytic chemistry of the supported Pd centers (vide supra), it is possible that higher treatment temperatures and prolonged reaction may contribute to the growth of larger and more numerous Pd sites with increased hydrogenation activity but decreased selectivity. Numerous investigations have focused on the effects of particle size and site-isolation in selective hydrogenations.[48,52−57] Notable examples include: single-site, supported Pd in enantioselective hydrogenation;[1] site-isolated Pd−Ga intermetallic compounds in selective acetylene hydrogenation;[58,59] and explorations into the role of subsurface hydrogen in alkyne hydrogenation.[60,61]

CONCLUSIONS

The tris(*tert*-butoxy)siloxy palladium complexes **1** and **2** were synthesized and fully characterized. These precursors were used

dx.doi.org/10.1021/cs2002719 |*ACS Catal.* 2011, 1, 1166–1177

to introduce well-defined, highly disperse Pd(II) centers onto the surface of SBA15 under mild conditions. The incorporation of the -OSi(O^tBu)$_3$ ligands in **1** and **2** facilitated their use as spectroscopic models for the supported Pd centers. The supported Pd(II) centers share many of the same structural and spectroscopic characteristics as the corresponding molecular precursors. The supported Pd centers were robust up to the decomposition temperatures of **1** and **2** (150−200 °C). X-ray absorption studies of the supported Pd(II) centers demonstrated that they remained site-isolated upon grafting at room temperature. At temperatures above 150 °C, Pd−Pd contributions in the extended region of the X-ray absorption spectra demonstrated that the Pd(II) centers begin to aggregrate to form small particles. These small particles were particularly difficult to reduce; the small (∼1.5 nm) Pd particles formed upon reduction in H_2 at 300 °C still had a significant (30%) Pd(II) contribution. Finally, in comparison with **1** and **2** in solution, the supported materials exhibited marked enhancements in stability and selectivity to (*Z*)-1-phenyl-1-propene in the semihydrogenation of 1-phenyl-1-propyne. Palladium is well-known to catalyze a wide variety of transformations, and therefore these TMP-derived materials offer the opportunity to investigate reactivity at a single, well-defined heterogeneous site.

■ ASSOCIATED CONTENT

Supporting Information. X-ray crystallographic data (and CIF files) for **1** and **2**, FTIR spectra of **1**, **Pd(1)SBA15**, **2** and **Pd(2)SBA15**, thermogravimetric data for **1** and **2** in O_2, adsorption−desorption data and the small-angle PXRD pattern for unmodified SBA15, original XANES and EXAFS plot for **Pd(1)SBA15** in He and hydrogen after various thermal treatments, tabular summary of XANES and EXAFS data fitting, PXRD patterns for **Pd(2)SBA15**, **Pd(2)SBA15$_{300}$**, **Pd(2)SBA15$_{400}$**, and **Pd(2)SBA15$_{500}$**, and catalytic hydrogenation data for **1**, **Pd(1)SBA15**, **2**, and **Pd(2)SBA15** after heat treatment in N_2 at various temperatures. This material is available free of charge via the Internet at http://pubs.acs.org.

■ AUTHOR INFORMATION

Corresponding Author

*E-mail: rioux@engr.psu.edu (R.M.R.), tdtilley@berkeley.edu (T.D.T.).

Funding Sources

The authors gratefully acknowledge the support of the Director, Office of Energy Research, Office of Basic Energy Sciences, Chemical Sciences Division, of the U.S. Department of Energy under contract DE-AC02-05CH11231. MRCAT operations are supported by the Department of Energy and the MRCAT member institutions.

■ ACKNOWLEDGMENT

The authors also gratefully acknowledge A. Paul Alivisatos at the University of California, Berkeley, for use of the PXRD and transmission electron microscope instruments.

■ REFERENCES

(1) Thomas, J. M.; Raja, R.; Lewis, D. W. *Angew. Chem., Int. Ed.* **2005**, *44*, 6456–6482.
(2) Coperet, C.; Chabanas, M.; Saint-Arroman, R. P.; Basset, J. M. *Angew. Chem., Int. Ed.* **2003**, *42*, 156–181.
(3) Comas-Vives, A.; Gonzalez-Arellano, C.; Corma, A.; Iglesias, M.; Sanchez, F.; Ujaque, G. *J. Am. Chem. Soc.* **2006**, *128*, 4756–4765.
(4) Corma, A.; Garcia, H. *Top. Catal.* **2008**, *48*, 8–31.
(5) Poli, G.; Giambastiani, G.; Heumann, A. *Tetrahedron* **2000**, *56*, 5959–5989.
(6) Stahl, S. S. *Angew. Chem., Int. Ed.* **2004**, *43*, 3400–3420.
(7) Hackett, S. E. J.; Brydson, R. M.; Gass, M. H.; Harvey, I.; Newman, A. D.; Wilson, K.; Lee, A. F. *Angew. Chem., Int. Ed.* **2007**, *46*, 8593–8596.
(8) Mori, K.; Hara, T.; Mizugaki, T.; Ebitani, K.; Kaneda, K. *J. Am. Chem. Soc.* **2004**, *126*, 10657–10666.
(9) Phan, N. T. S.; Van Der Sluys, M.; Jones, C. W. *Adv. Synth. Catal.* **2006**, *348*, 609–679.
(10) Fujdala, K. L.; Drake, I. J.; Bell, A. T.; Tilley, T. D. *J. Am. Chem. Soc.* **2004**, *126*, 10864–10866.
(11) Mandal, S.; Roy, D.; Chaudhari, R. V.; Sastry, M. *Chem. Mater.* **2004**, *16*, 3714–3724.
(12) Ruddy, D. A.; Ohler, N. L.; Bell, A. T.; Tilley, T. D. *J. Catal.* **2006**, *238*, 277–285.
(13) Ruddy, D. A.; Tilley, T. D. *Chem. Commun.* **2007**, 3350–3352.
(14) Corma, A.; Garcia, H. *Adv. Synth. Catal.* **2006**, *348*, 1391–1412.
(15) Brutchey, R. L.; Drake, I. J.; Bell, A. T.; Tilley, T. D. *Chem. Commun.* **2005**, 3736–3738.
(16) Fujdala, K. L., Brutchey, R. L., Tilley, T. D. In *Surface and Interfacial Organometallic Chemistry and Catalysis*; Copéret, C., Chaudret, B., Eds.; Springer: Berlin, Germany, 2005; Vol. 16, pp 69−115.
(17) Fujdala, K. L.; Tilley, T. D. *J. Am. Chem. Soc.* **2001**, *123*, 10133–10134.
(18) Ruddy, D. A.; Jarupatrakorn, J.; Rioux, R. M.; Miller, J. T.; McMurdo, M. J.; McBee, J. L.; Tupper, K. A.; Tilley, T. D. *Chem. Mater.* **2008**, *20*, 6517–6527.
(19) Jarupatrakorn, J.; Coles, M. P.; Tilley, T. D. *Chem. Mater.* **2005**, *17*, 1818–1828.
(20) Jarupatrakorn, J.; Tilley, T. D. *Dalton Trans.* **2004**, 2808–2813.
(21) Degraaf, W.; Boersma, J.; Smeets, W. J. J.; Spek, A. L.; Vankoten, G. *Organometallics* **1989**, *8*, 2907–2917.
(22) Abe, Y.; Kijima, I. *Bull. Chem. Soc. Jpn.* **1969**, *42*, 1118.
(23) Terry, K. W.; Su, K.; Tilley, T. D.; Rheingold, A. L. *Polyhedron* **1998**, *17*, 891–897.
(24) Zhang, H.; Sun, J. M.; Ma, D.; Bao, X. H.; Klein-Hoffmann, A.; Weinberg, G.; Su, D. S.; Schlogl, R. *J. Am. Chem. Soc.* **2004**, *126*, 7440–7441.
(25) Brunauer, S.; Emmett, P. H.; Teller, E. *J. Am. Chem. Soc.* **1938**, *60*, 309–319.
(26) Barrett, E. P.; Joyner, L. G.; Halenda, P. P. *J. Am. Chem. Soc.* **1951**, *73*, 373–380.
(27) Ressler, T. *J. Phys. IV* **1997**, *7*, 269–270.
(28) Qin, Z. Q.; Jennings, M. C.; Puddephatt, R. J. *Inorg. Chem.* **2002**, *41*, 3967–3974.
(29) Degraaf, W.; Boersma, J.; Vankoten, G. *Organometallics* **1990**, *9*, 1479–1484.
(30) Wehman, P.; Dol, G. C.; Moorman, E. R.; Kamer, P. C. J.; Vanleeuwen, P.; Fraanje, J.; Goubitz, K. *Organometallics* **1994**, *13*, 4856–4869.
(31) Kapteijn, G. M.; Grove, D. M.; Kooijman, H.; Smeets, W. J. J.; Spek, A. L.; vanKoten, G. *Inorg. Chem.* **1996**, *35*, 526–533.
(32) Gong, Y. Q.; Cheng, Y. F.; Gu, J. M.; Hu, X. R. *Polyhedron* **1997**, *16*, 3743–3746.
(33) Paul, F.; Fischer, J.; Ochsenbein, P.; Osborn, J. A. *Organometallics* **1998**, *17*, 2199–2206.
(34) Mintcheva, N.; Tanabe, M.; Osakada, K. *Organometallics* **2007**, *26*, 1402–1410.
(35) Tanabe, M.; Mutou, K.; Mintcheva, N.; Osakada, K. *Organometallics* **2008**, *27*, 519–523.
(36) Ruiz, J.; Vicente, C.; Rodriguez, V.; Cutillas, N.; Lopez, G.; de Arellano, C. R. *J. Organomet. Chem.* **2004**, *689*, 1872–1875.

(37) Terry, K. W.; Lugmair, C. G.; Gantzel, P. K.; Tilley, T. D. *Chem. Mater.* **1996**, *8*, 274–280.
(38) Teranishi, T.; Miyake, M. *Chem. Mater.* **1998**, *10*, 594–600.
(39) Boudart, M.; Hwang, H. S. *J. Catal.* **1975**, *39*, 44–52.
(40) McCaulley, J. A. *J. Phys. Chem.* **1993**, *97*, 10372–10379.
(41) Davis, R. J.; Landry, S. M.; Horsley, J. A.; Boudart, M. *Phys. Rev. B* **1989**, *39*, 10580–10583.
(42) Tew, M. W.; Miller, J. T.; van Bokhoven, J. A. *J. Phys. Chem. C* **2009**, *113*, 15140–15147.
(43) Benson, J. E.; Hwang, H. S.; Boudart, M. *J. Catal.* **1973**, *30*, 146–153.
(44) Greegor, R. B.; Lytle, F. W. *J. Catal.* **1980**, *63*, 476–486.
(45) Yu, J. Q.; Whitney, P. S.; Spencer, J. B. *J. Mol. Catal. A: Chem.* **1999**, *146*, 199–210.
(46) Marin-Astorga, N.; Pecchi, G.; Pinnavaia, T. J.; Alvez-Manoli, G.; Reyes, P. *J. Mol. Catal. A: Chem.* **2006**, *247*, 145–152.
(47) Horiuti, I.; Polanyi, M. *Faraday Trans.* **1934**, *30*, 1164–1172.
(48) Dominguez-Dominguez, S.; Berenguer-Murcia, A.; Linares-Solano, A.; Cazorla-Amoros, D. *J. Catal.* **2008**, *257*, 87–95.
(49) Quiroga, M. E.; Liprandi, D. A.; Cagnola, E. A.; Argentiere, P. C. L. *Appl. Catal., A* **2007**, *326*, 121–129.
(50) Semagina, N.; Joannet, E.; Parra, S.; Sulman, E.; Renken, A.; Kiwi-Minsker, L. *Appl. Catal., A* **2005**, *280*, 141–147.
(51) Crespo-Quesada, M.; Dykeman, R. R.; Laurenczy, G.; Dyson, P. J.; Kiwi-Minsker, L. *J. Catal.* **2011**, *279*, 66–74.
(52) Bhattacharjee, S.; Dotzauer, D. M.; Bruening, M. L. *J. Am. Chem. Soc.* **2009**, *131*, 3601–3610.
(53) Panpranot, J.; Pattamakomsan, K.; Praserthdam, P.; Goodwin, J. G. *Ind. Eng. Chem. Res.* **2004**, *43*, 6014–6020.
(54) Singh, U. K.; Vannice, M. A. *Appl. Catal., A* **2001**, *213*, 1–24.
(55) Alvez-Manoli, G.; Pinnavaia, T. J.; Zhang, Z.; Lee, D. K.; Marin-Astorga, K.; Rodriguez, P.; Imbert, F.; Reyes, P.; Marin-Astorga, N. *Appl. Catal., A* **2010**, *387*, 26–34.
(56) Stakheev, A.; Mashkovskii, I.; Baeva, G.; Telegina, N. *Russ. J. Gen. Chem.* **2010**, *80*, 618–629.
(57) Hori, J.; Murata, K.; Sugai, T.; Shinohara, H.; Noyori, R.; Arai, N.; Kurono, N.; Ohkuma, T. *Adv. Synth. Catal.* **2009**, *351*, 3143–3149.
(58) Osswald, J.; Giedigkeit, R.; Jentoft, R. E.; Armbruster, M.; Girgsdies, F.; Kovnir, K.; Ressler, T.; Grin, Y.; Schlogl, R. *J. Catal.* **2008**, *258*, 210–218.
(59) Osswald, J.; Kovnir, K.; Armbruster, M.; Giedigleit, R.; Jentoft, R. E.; Wild, U.; Grin, Y.; Schlogl, R. *J. Catal.* **2008**, *258*, 219–227.
(60) Doyle, A. M.; Shaikhutdinov, S. K.; Jackson, S. D.; Freund, H. J. *Angew. Chem., Int. Ed.* **2003**, *42*, 5240–5243.
(61) Teschner, D.; Borsodi, J.; Wootsch, A.; Revay, Z.; Havecker, M.; Knop-Gericke, A.; Jackson, S. D.; Schlogl, R. *Science* **2008**, *320*, 86–89.